

## Development of Colorimetric Sensor Utilizing Itaconic Acid-mediated Griess Reaction for Sensitive Detection of Nitrite and Nitrate in Agricultural Products

Anubhab Das,<sup>a</sup> Sindhu I Sanakal,<sup>a</sup> Gomathi Sivakumar,<sup>a</sup> Anashwara Babu<sup>a</sup> and Samarendra Maji\*<sup>a</sup>

<sup>a</sup>Department of Chemistry, Faculty of Engineering and Technology, SRM Institute of Science and Technology (SRMIST), Kattankulathur, Tamil Nadu-603203, India.

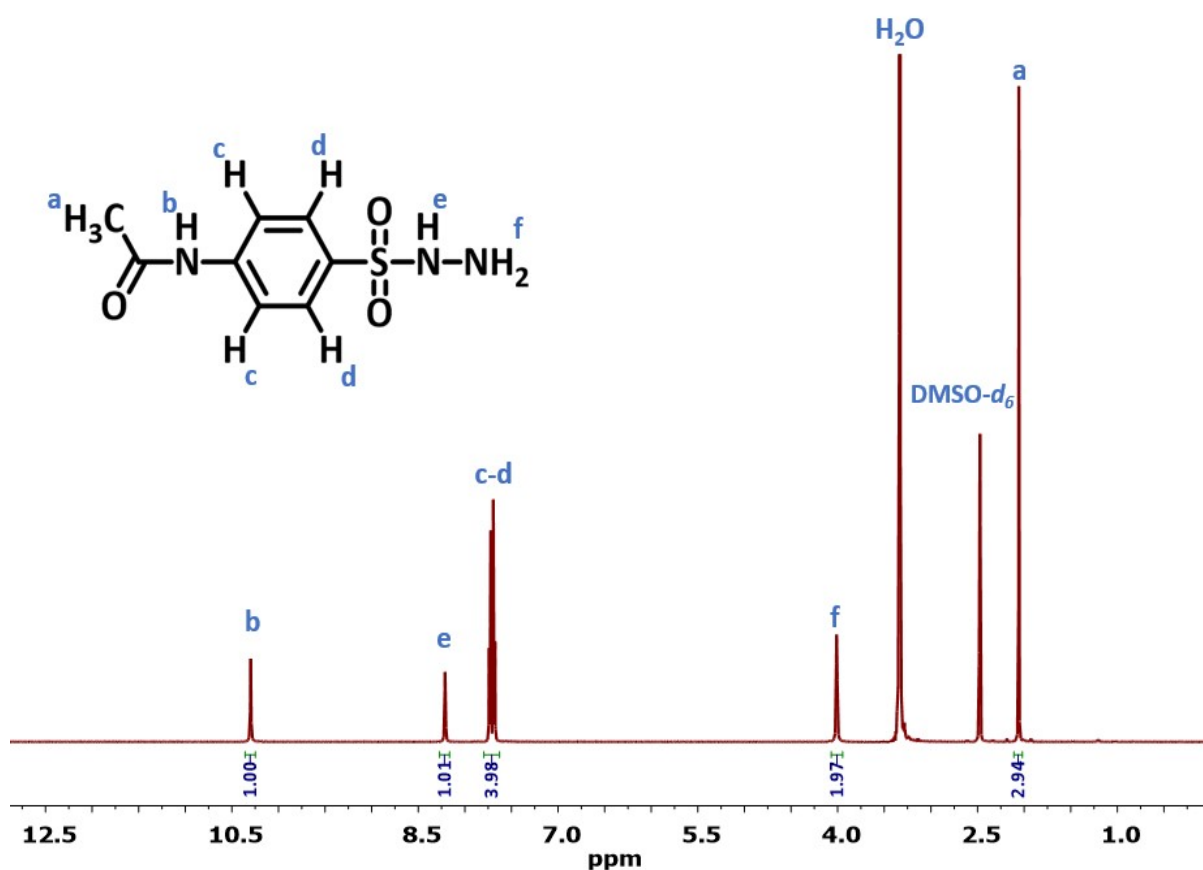


Figure S1. <sup>1</sup>H NMR spectrum of the compound (B).

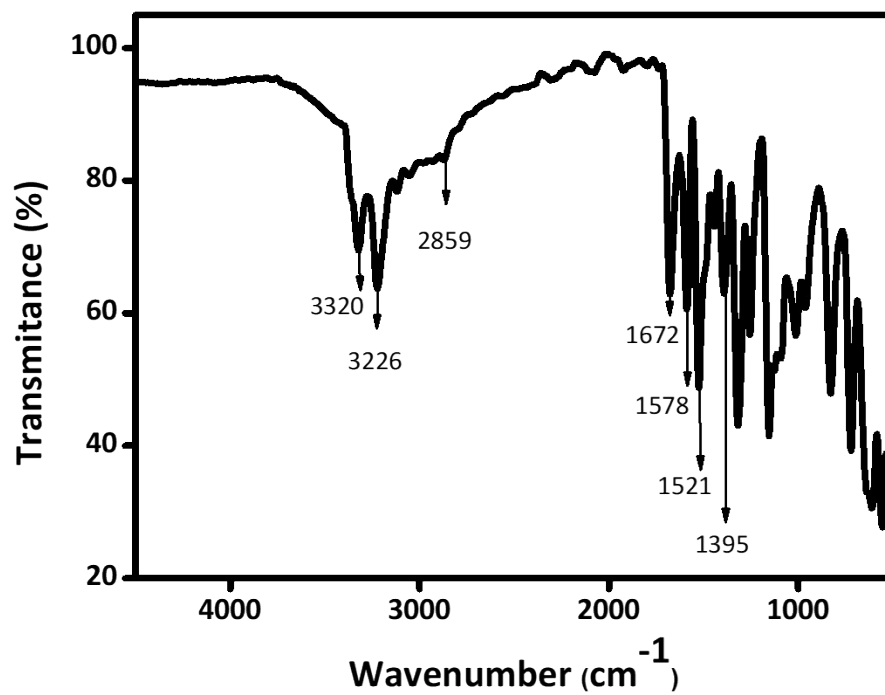


Figure S2. FTIR spectrum of compound (B).

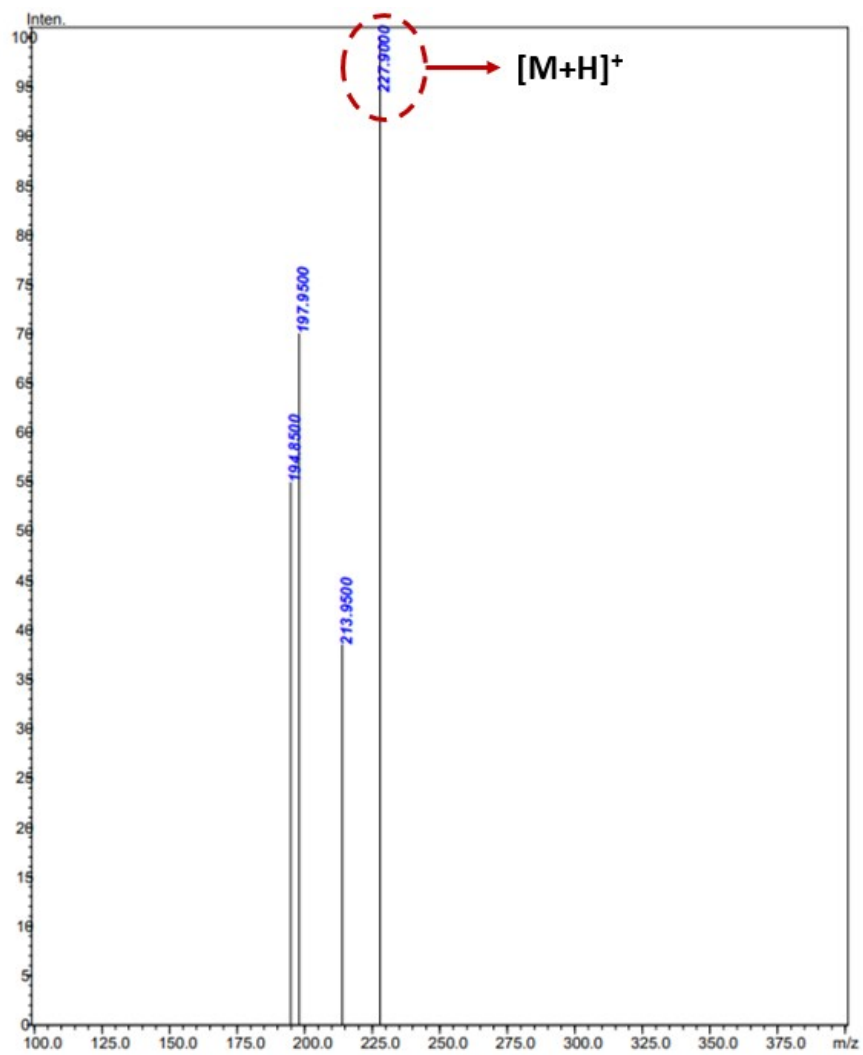


Figure S3. LC-MS spectrum of compound (B).

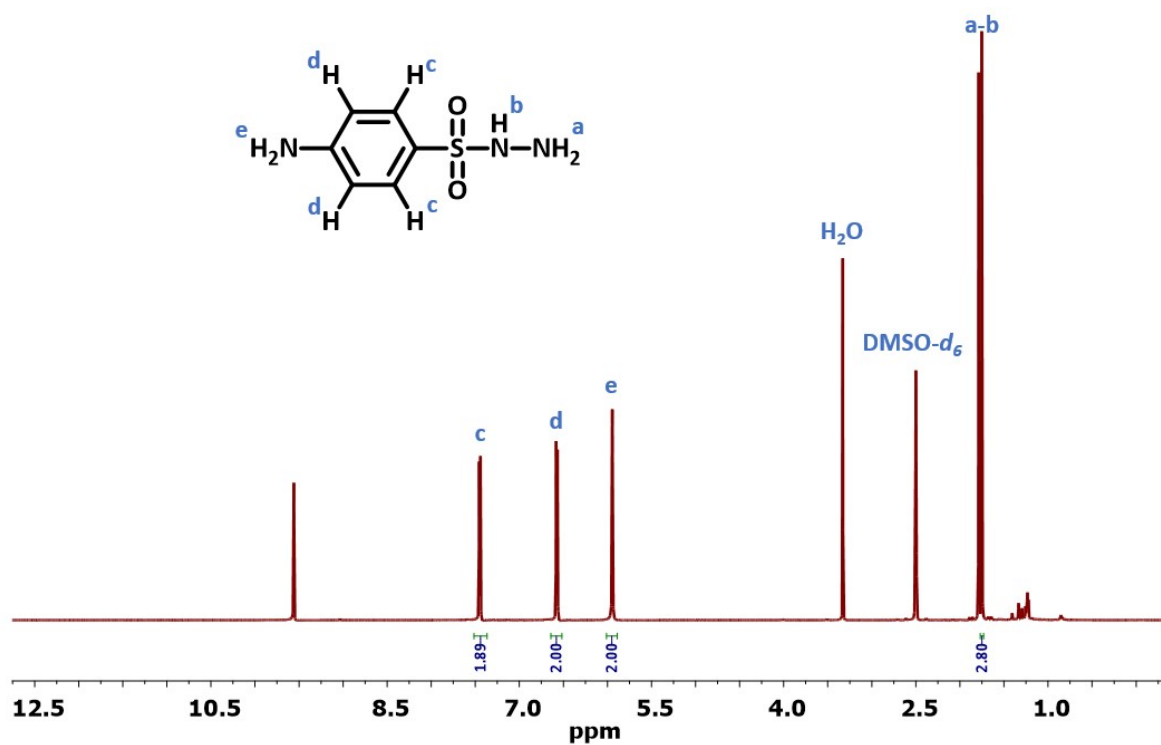


Figure S4. <sup>1</sup>H NMR spectrum of the compound (C).

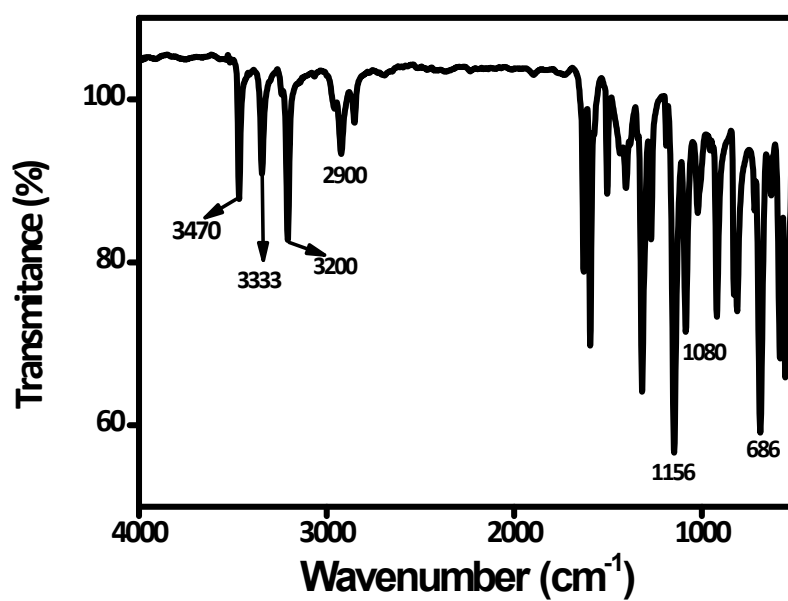


Figure S5. FTIR spectrum of compound (C).

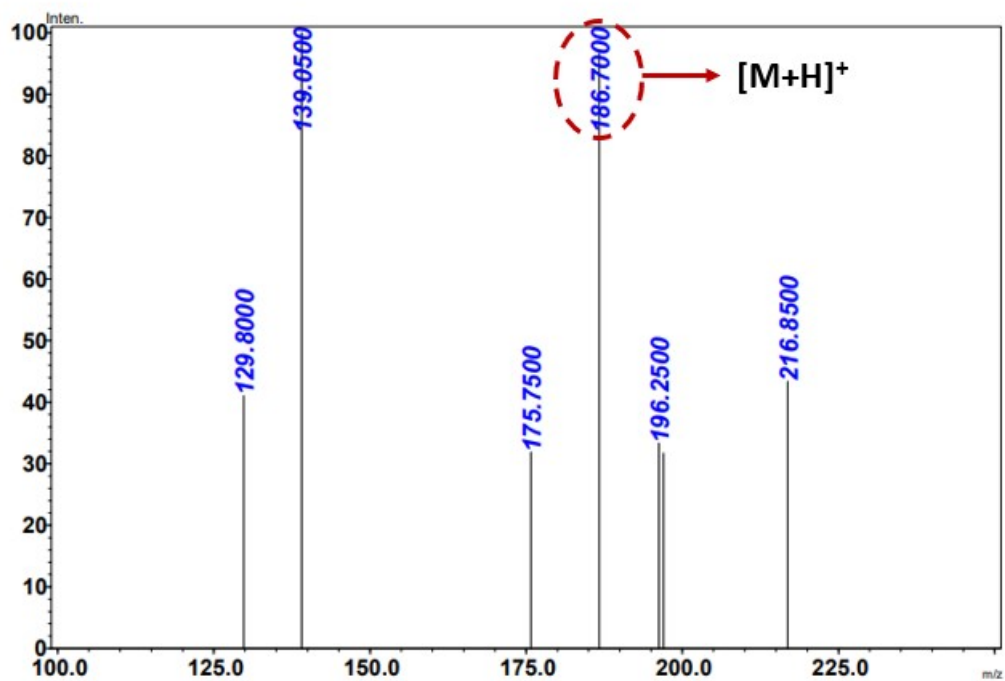


Figure S6. LC-MS spectrum of compound (C).

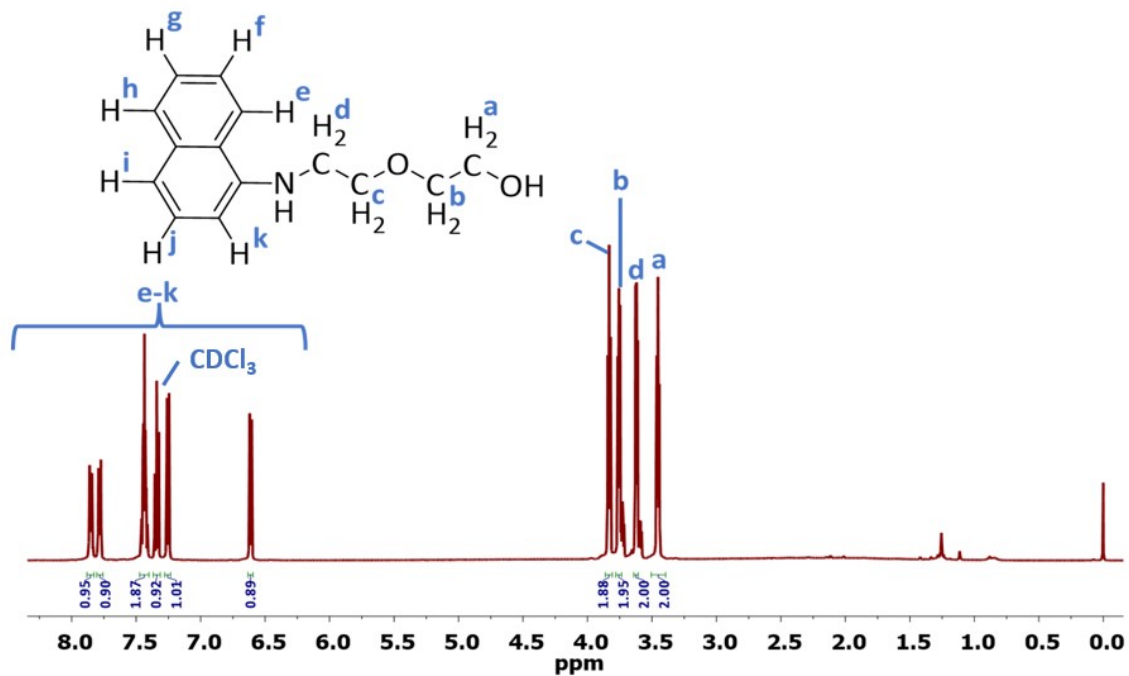


Figure S7. <sup>1</sup>H NMR spectrum of the compound (E).

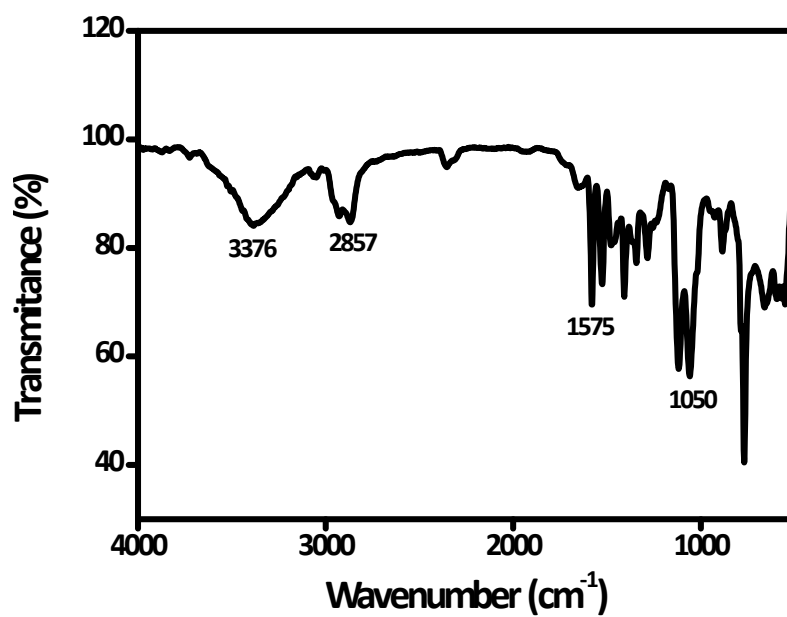


Figure S8. FTIR spectrum of compound (E).

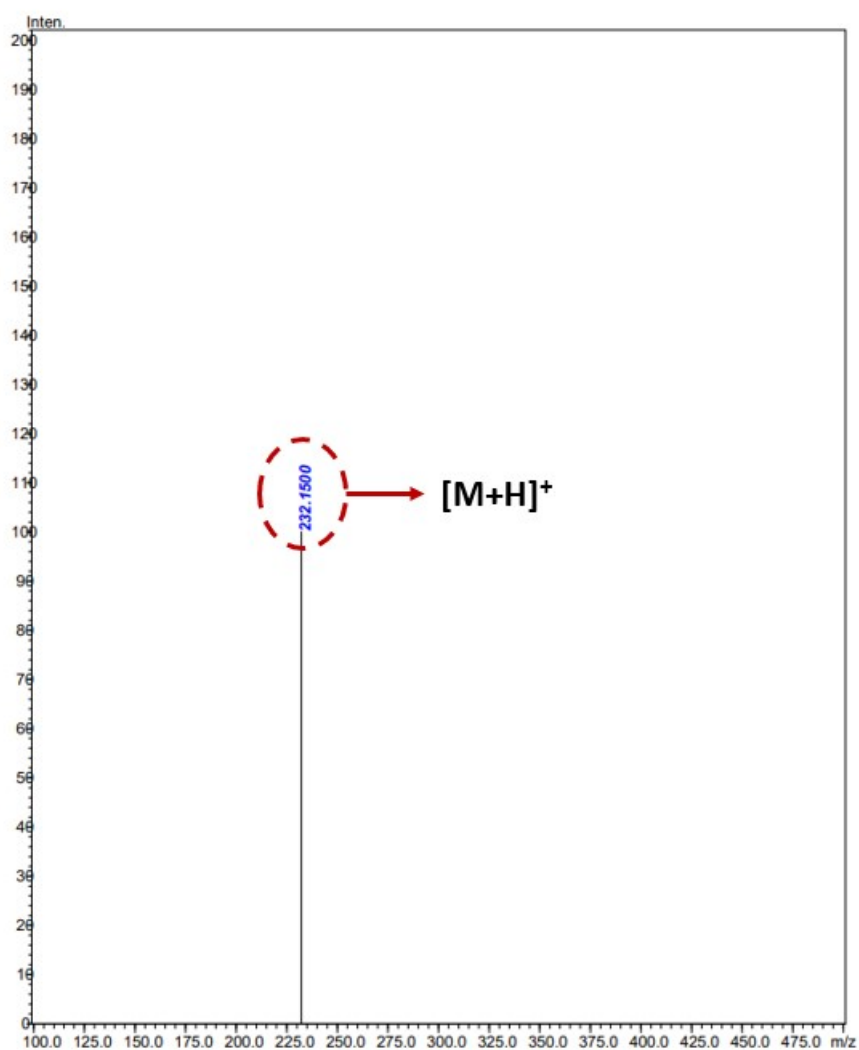
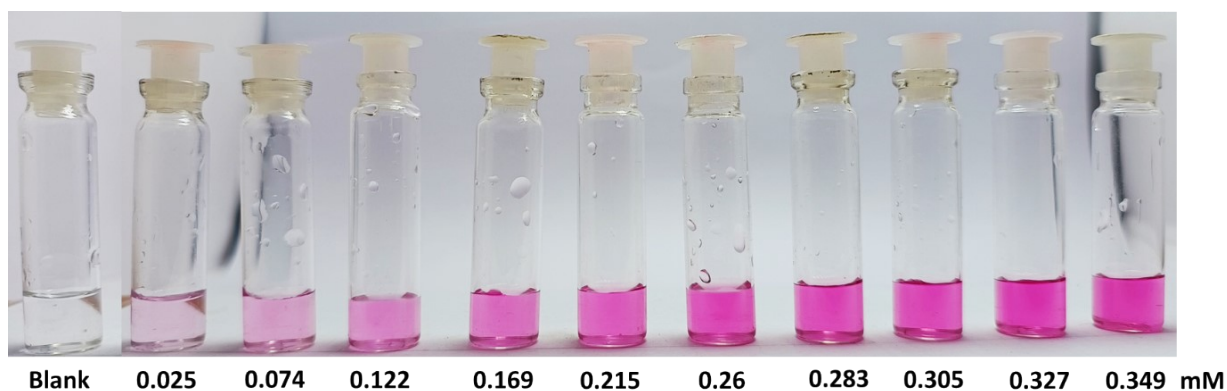
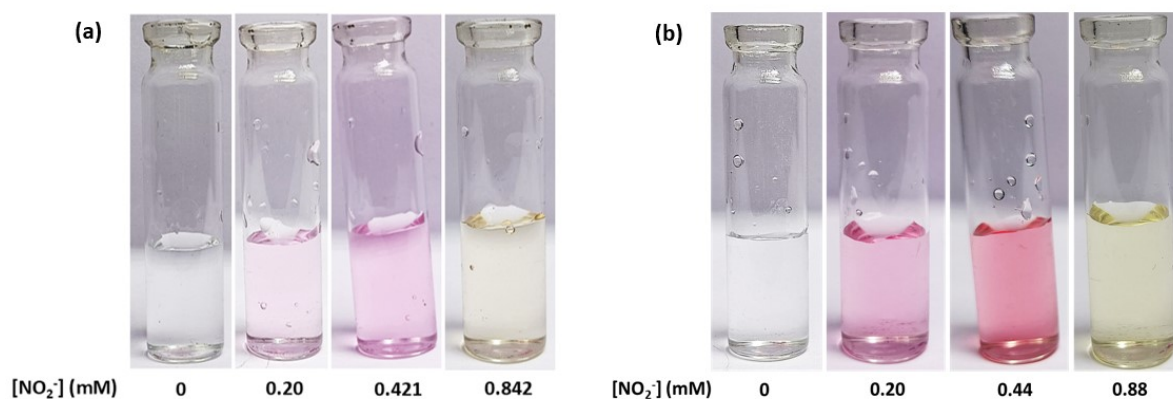


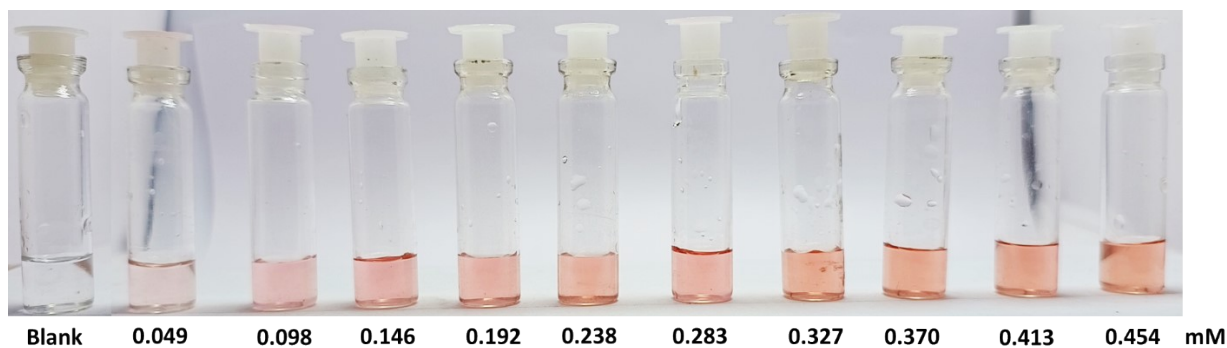
Figure S9. LC-MS spectrum of compound (E).



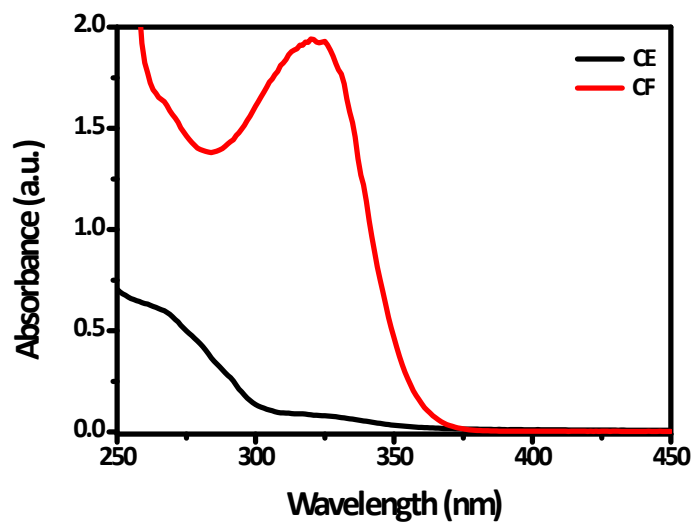
**Figure S10.** Visual performance of sensor (CE) with different concentrations (0.025-0.349 mM) of  $\text{NO}_2^-$  ion (concentration of each dye is 0.33 mM and concentration of itaconic acid is 2.66 mM).



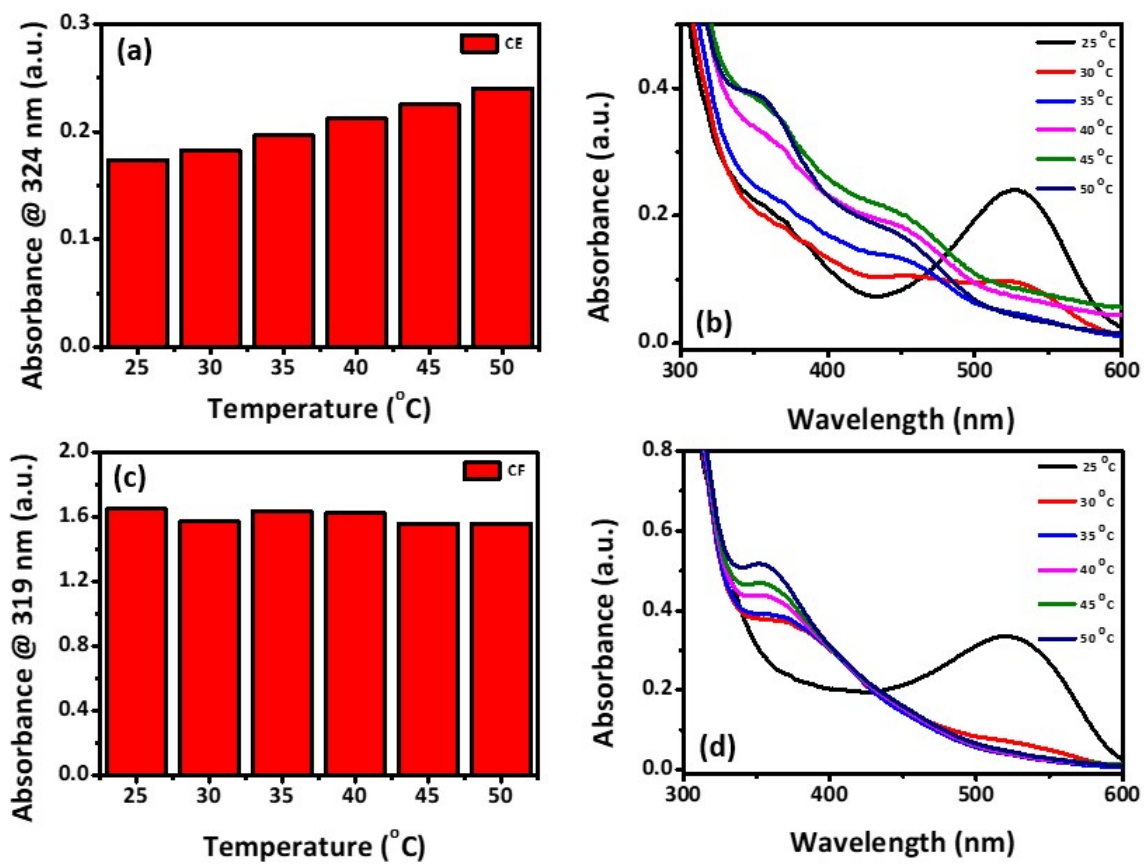
**Figure S11.** Displaying the visual color change of chemosensor (a) (CE) and (b) (CF) with different concentrations of nitrite (concentration of each dye is 0.25 mM and concentration of itaconic acid is 2.5 mM).



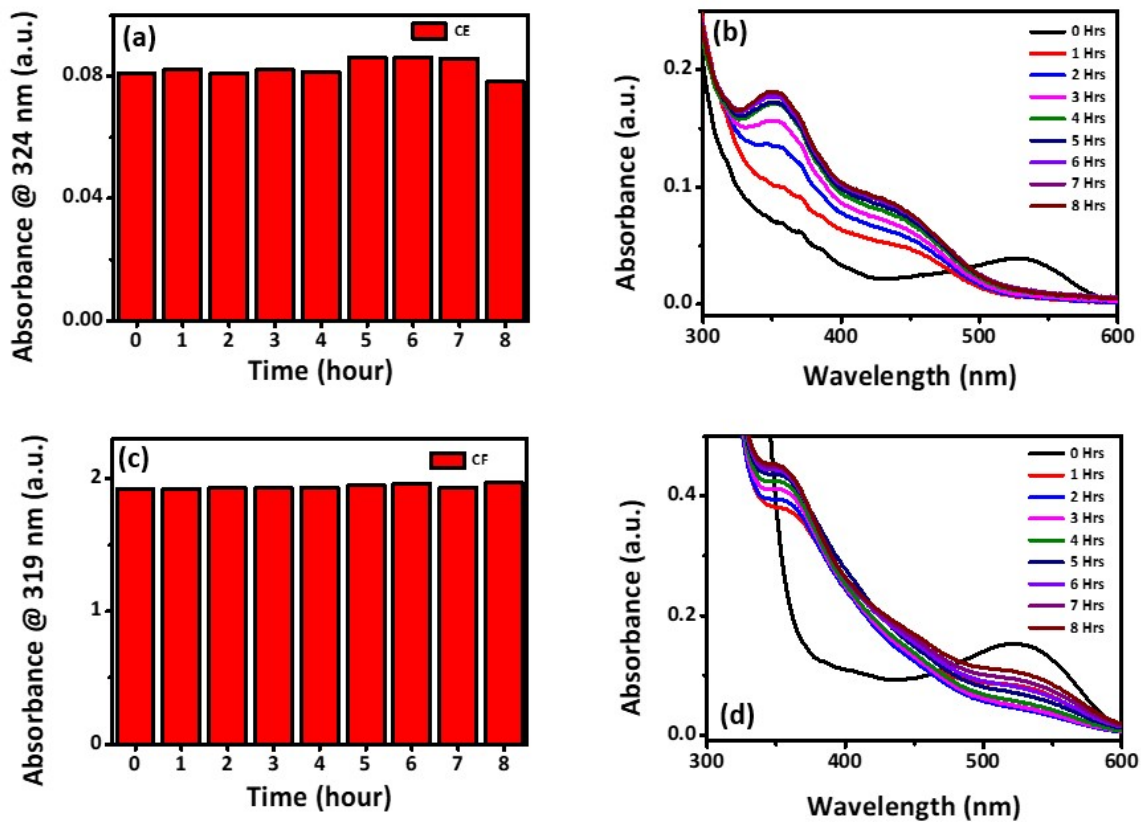
**Figure S12.** Visual performance of sensor (CF) with different concentrations (0.049-0.454 mM) of  $\text{NO}_2^-$  ion (concentration of each dye is 0.33 mM and concentration of itaconic acid is 2.66 mM).



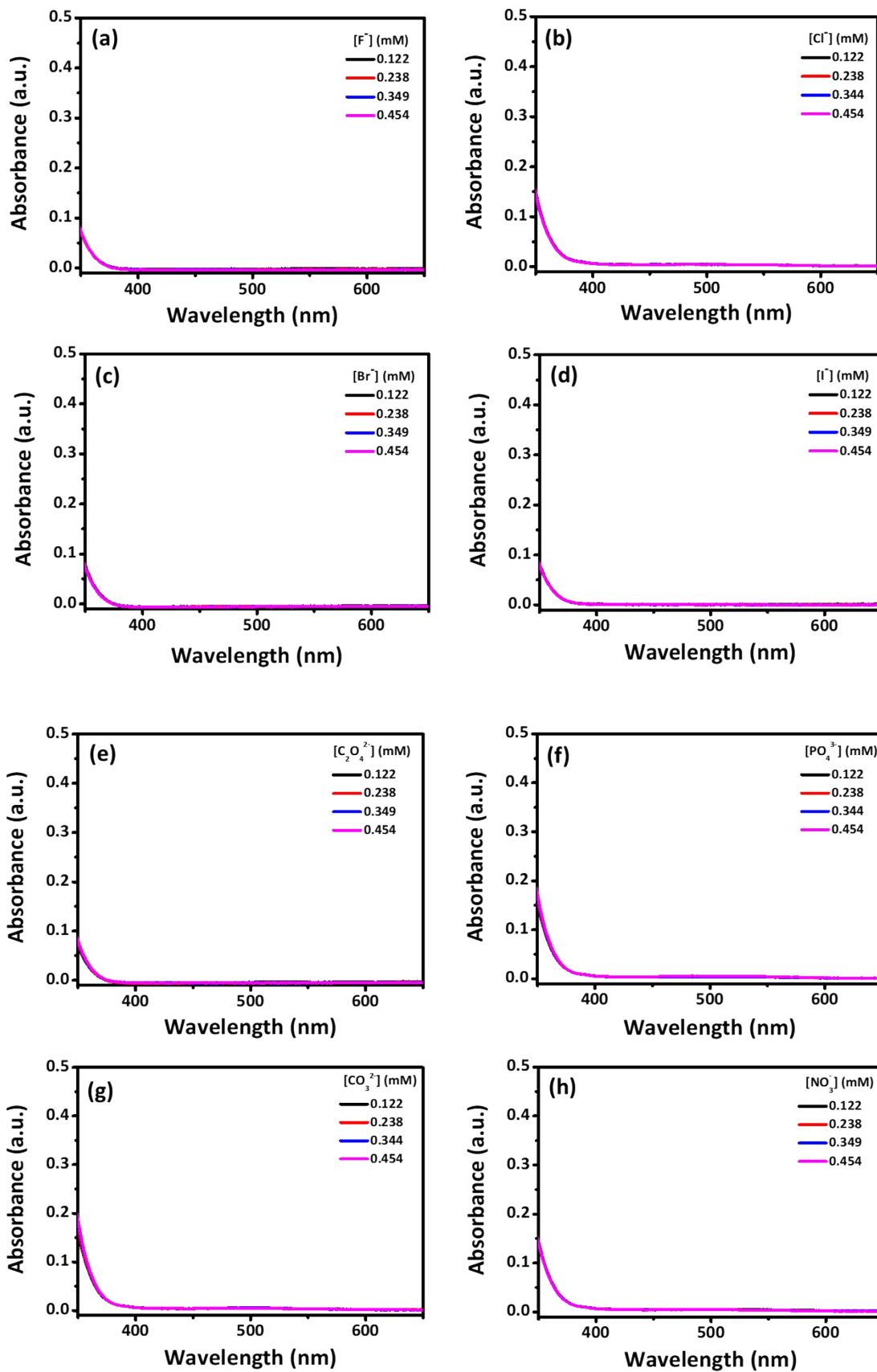
**Figure S13.** UV-Vis spectra of chemosensors (CE) and (CF) in the absence of nitrite.

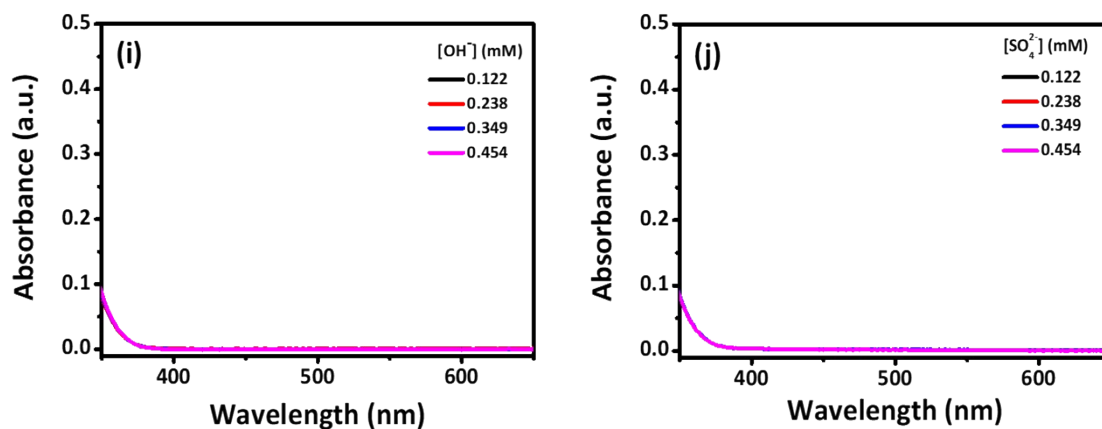


**Figure S14.** Temperature stability assessment 25 to 50 °C for (a) chemosensor CE, (b) nitrite responsive peak of sensor (CE), (c) chemosensor CF and (d) nitrite responsive peak of sensor (CF).

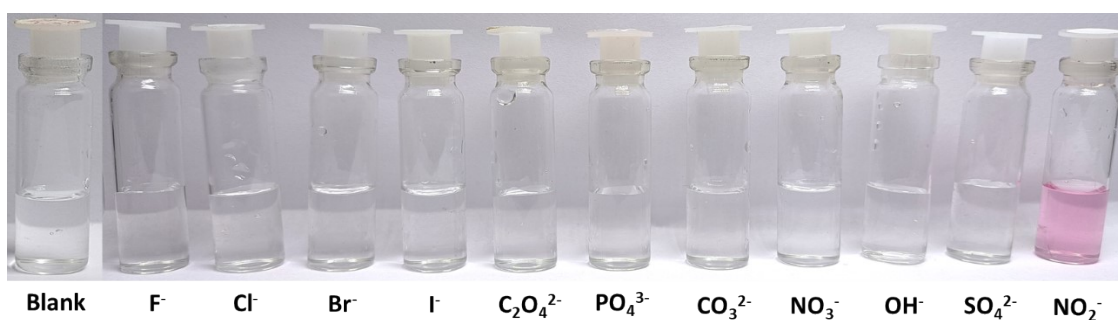


**Figure S15.** Prolonged stability over 0-8 hours for (a) chemosensor CE, (b) nitrite responsive peak of sensor (CE), (c) chemosensor CF, and (d) nitrite responsive peak of sensor (CF) @ 25 °C.

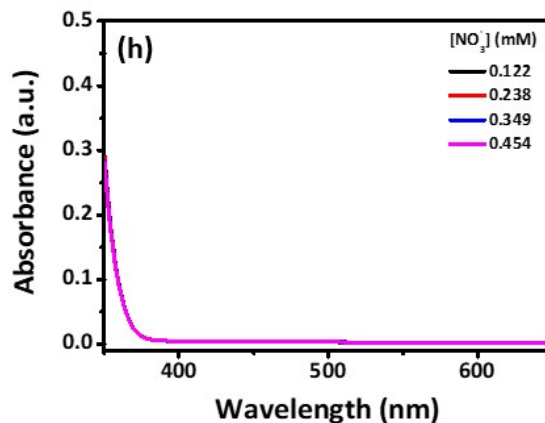
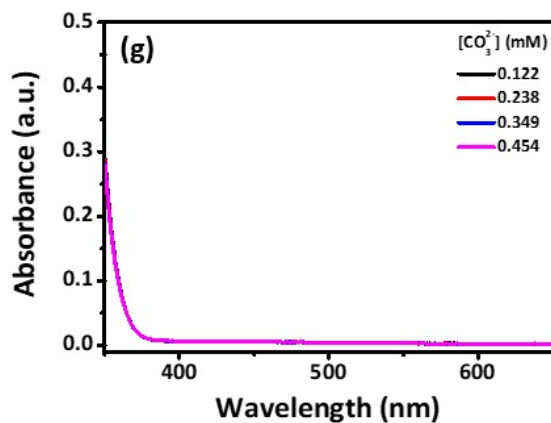
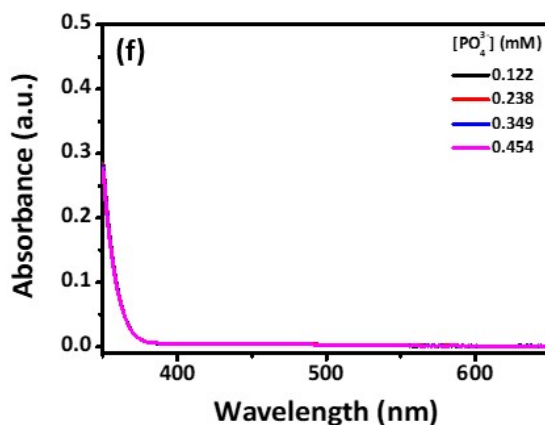
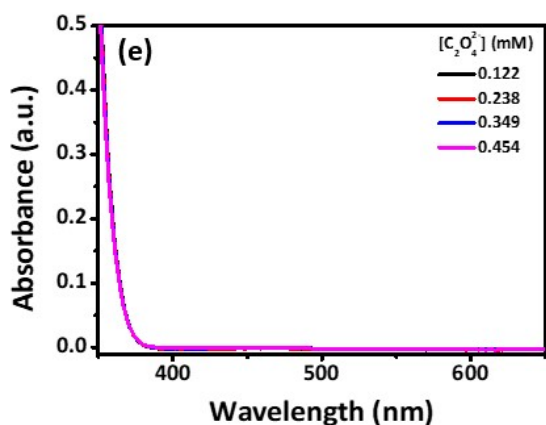
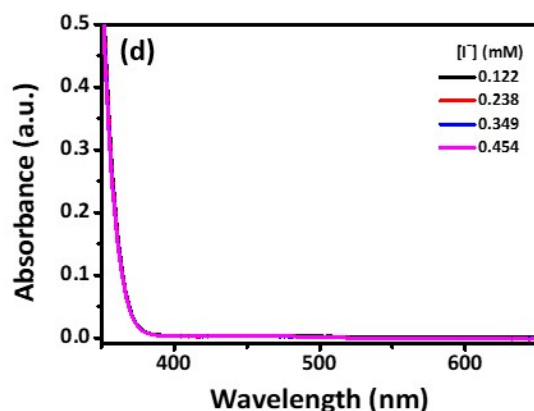
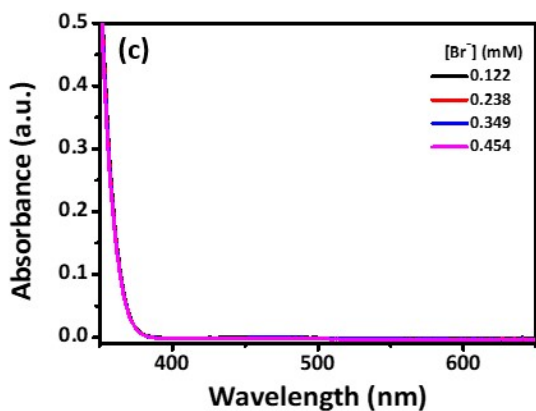
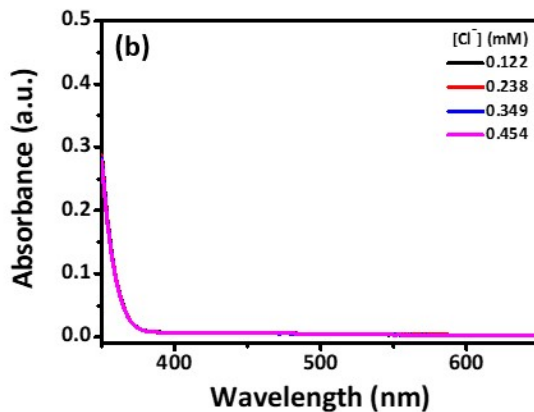
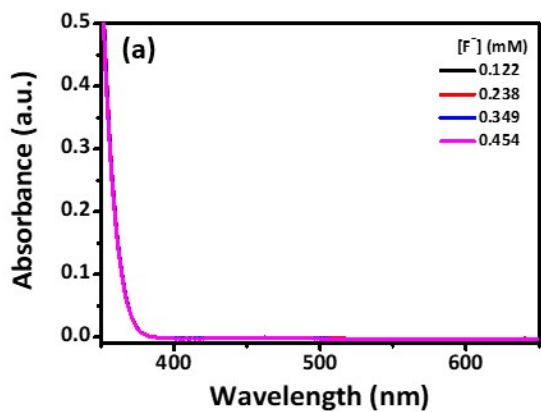




**Figure S16.** UV-vis spectra of a sensor (CE) in the presence of (a)  $F^-$ , (b)  $Cl^-$ , (c)  $Br^-$ , (d)  $I^-$ , (e)  $C_2O_4^{2-}$ , (f)  $PO_4^{3-}$ , (g)  $CO_3^{2-}$ , (h)  $NO_3^-$ , (i)  $OH^-$  and (j)  $SO_4^{2-}$  with different concentrations.



**Figure S17.** Naked eye color change of the sensor (CE) upon the addition of different anions (the concentration of each dye is 0.238 mM; the concentration of acid is 2.38 mM and the concentration of every anion is 0.238 mM).



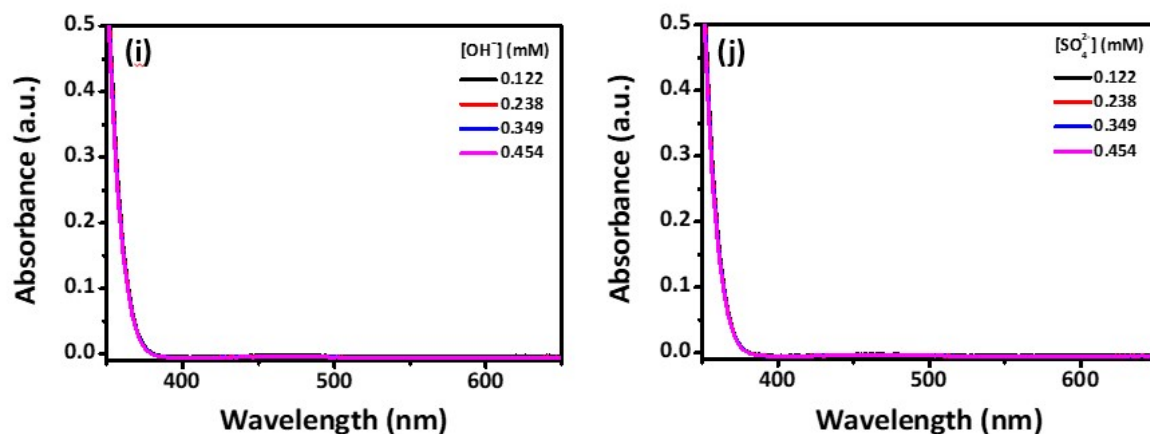


**Figure S18.** UV-Vis spectra of the sensor (CF) in the presence of (a)  $F^-$ , (b)  $Cl^-$ , (c)  $Br^-$ , (d)  $I^-$ , (e)  $C_2O_4^{2-}$ , (f)  $PO_4^{3-}$ , (g)  $CO_3^{2-}$ , (h)  $NO_3^-$ , (i)  $OH^-$  and (j)  $SO_4^{2-}$  with different concentrations.

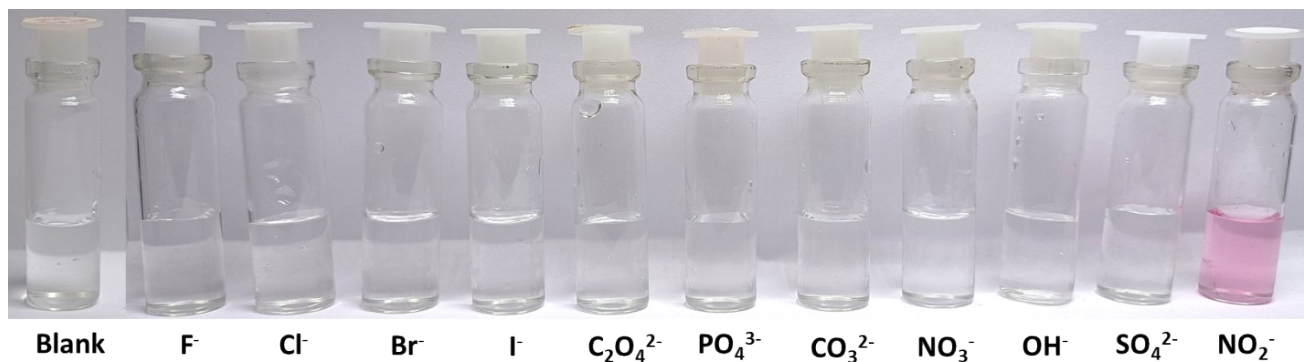


**Figure S19.** Naked eye color change of the sensor (CF) upon the addition of different anions (the concentration of dye is 0.238 mM; the concentration of acid is 2.38 mM and the concentration of anion is 0.238 mM).

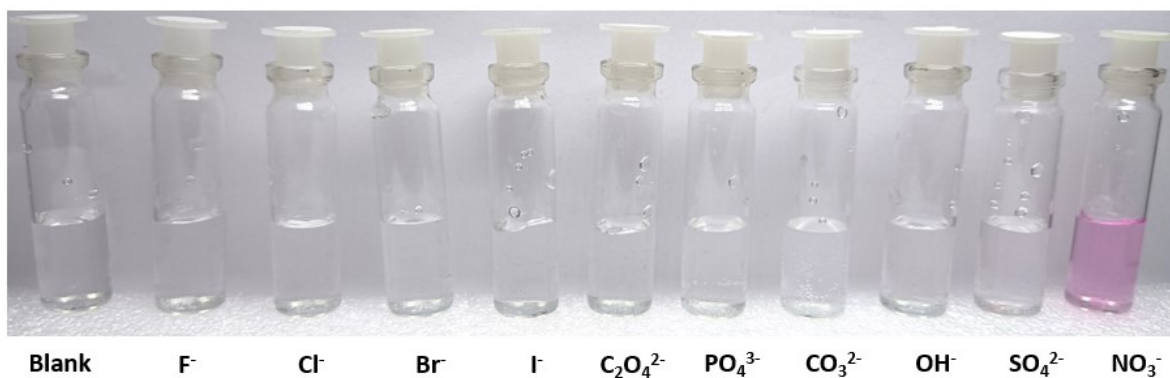


**Figure S20.** Naked eye color change of the sensor (CE) upon addition of different anions (the concentration of dye is 0.238 mM; the concentration of HCl is 2.5 mM. the concentration of anion is 0.238 mM and the concentration of Zn dust 1 mg/2 mL).

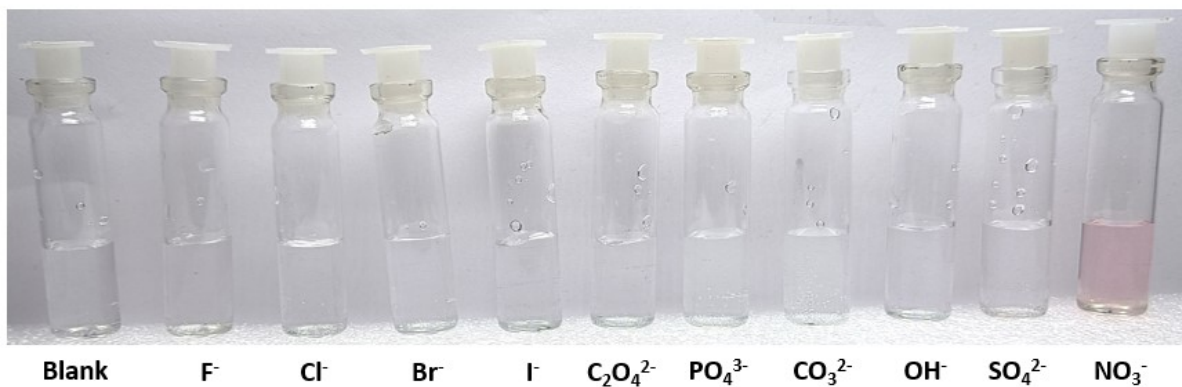


**Figure S21.** Naked eye color change of the sensor (CF) upon addition of different anions (the concentration of dye is 0.238 mM; the concentration of acid is 2.5 mM, the concentration of anion is 0.238 mM and the concentration of Zn dust 1 mg/2 mL).

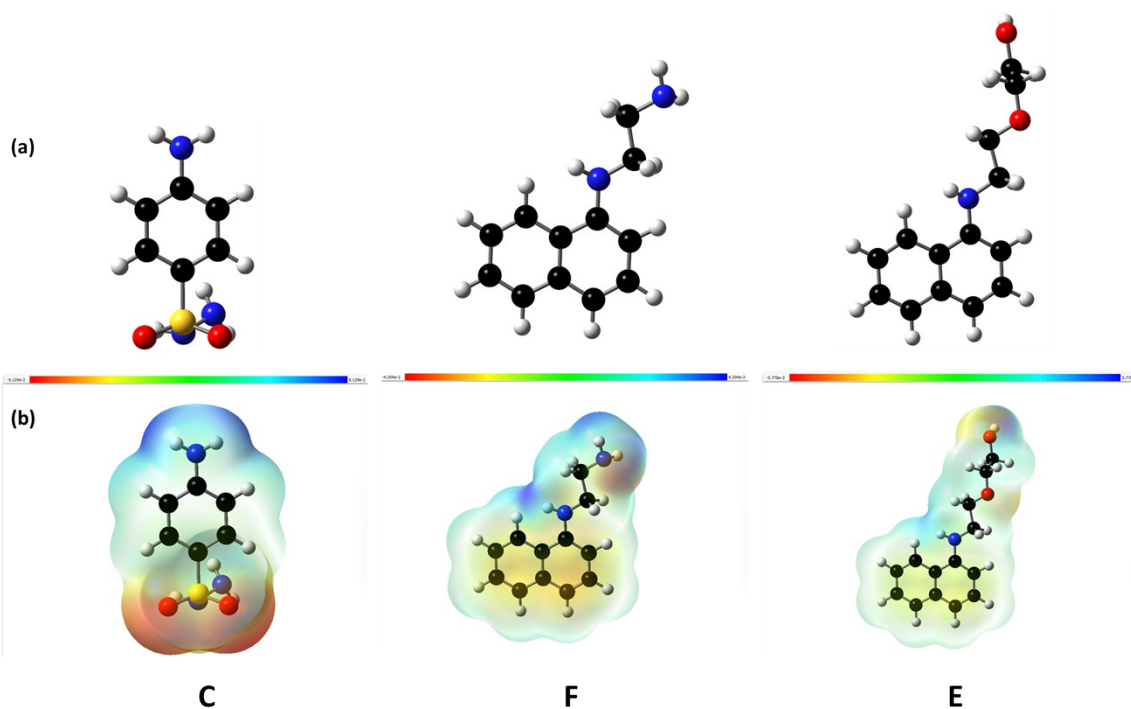


**Figure S22.** (a) Optimized structure and (b) Calculated electrostatic surfaces of compounds (C), (F) and (E).

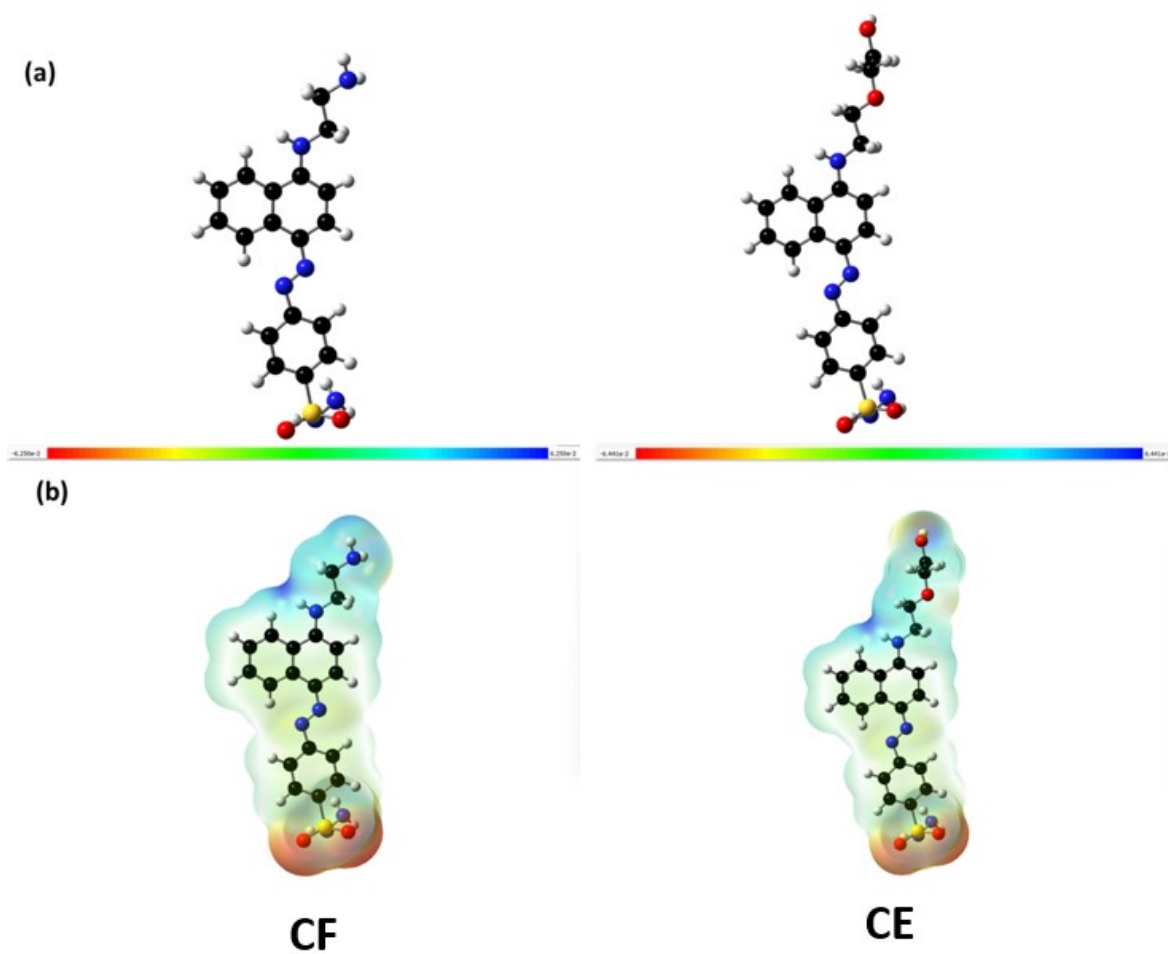


**Figure S23.** (a) Optimized structure and (b) Calculated electrostatic surfaces of azo dye (CF) and (CE).

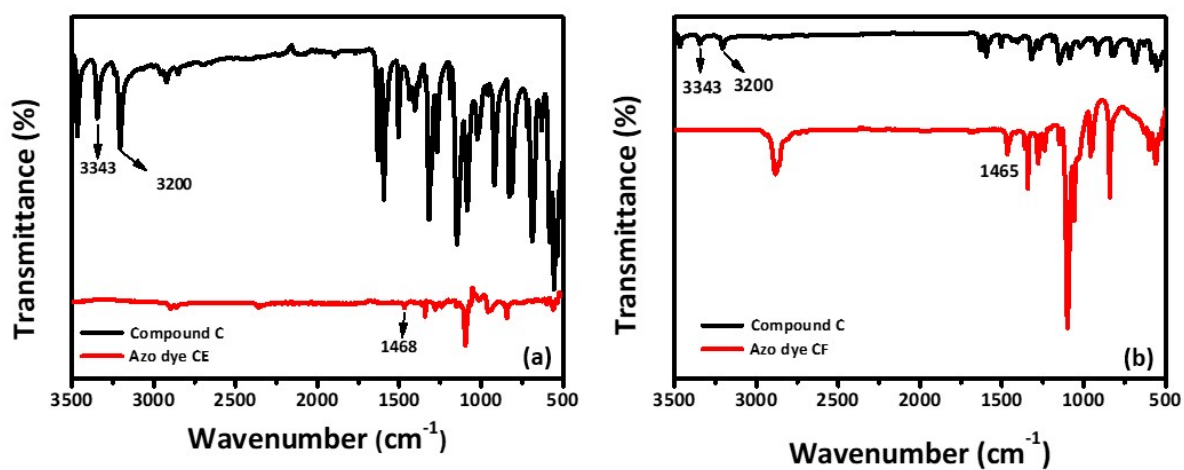


**Figure S24.** FT-IR spectra of (a) compound (C) and azo dye (CE), (b) compound (C) and azo dye (CF).

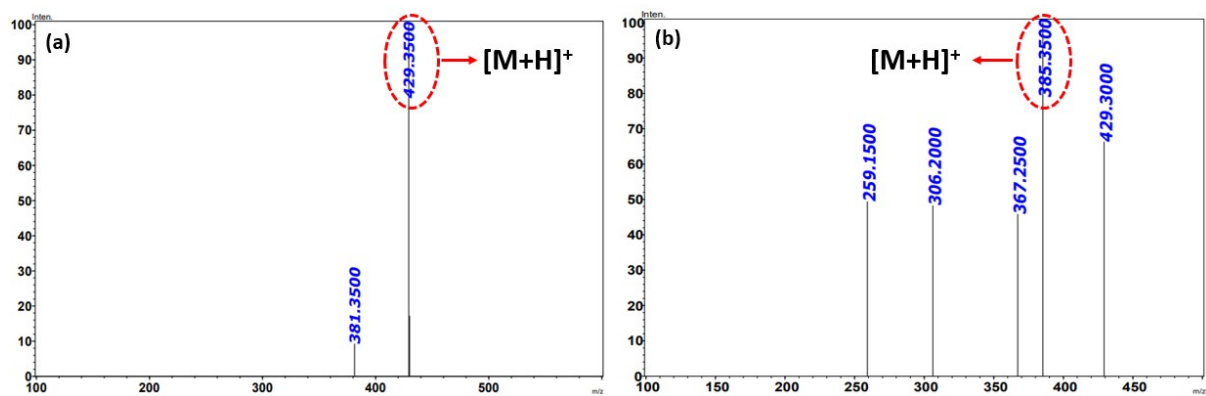


**Figure S25.** LC-MS spectra of azo-dyes (a) CE and (b) CF.

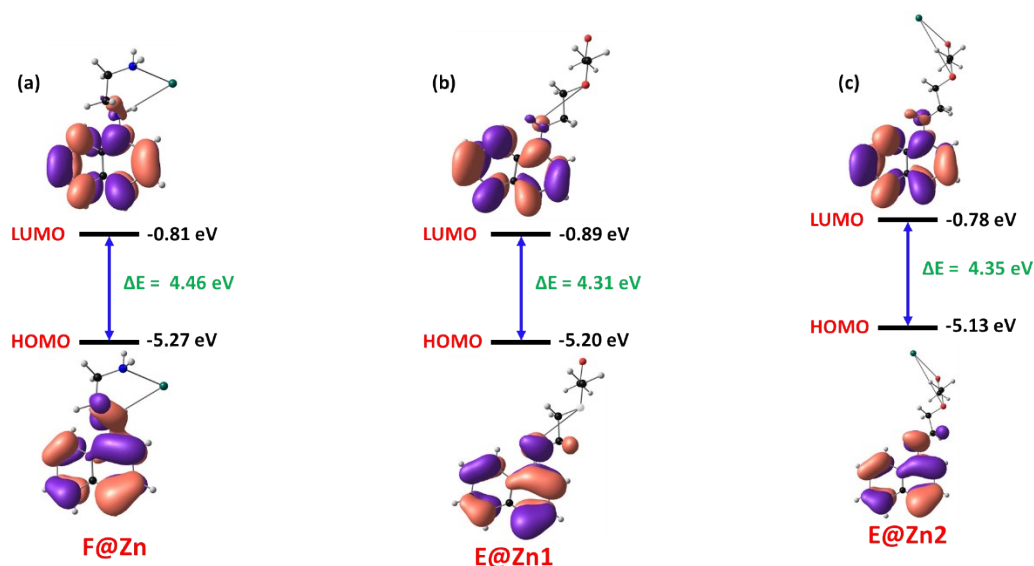


**Figure S26.** Energy profile diagram of Zn complex with (a) (F), (b) (E) (with bidentate ligand N and O), and (c) (E) (with bidentate ligand O and O).

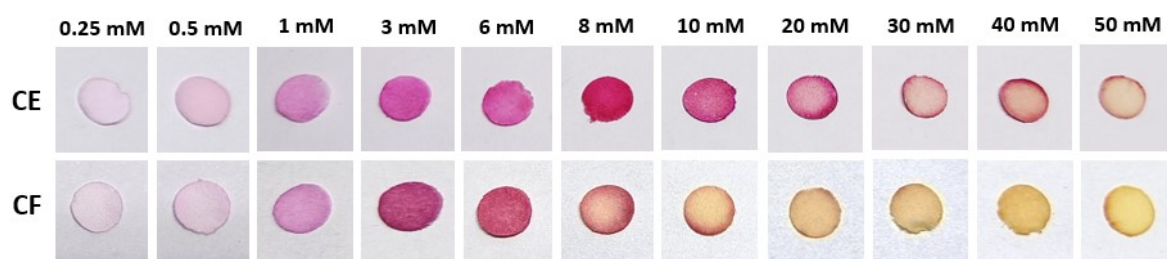


**Figure S27.** Photograph of sensing with test strips for sensor (CE) and (CF) in the presence of different concentrations of  $\text{NO}_2^-$ .

**Table S1.** Application of the colorimetric readout of a sensor system for the determination of  $\text{NO}_2^-$  in real samples spiked with different amounts of  $\text{NO}_2^-$ .

Samples	Added	For sensor CE		For sensor CF	
		Found	Recovery (%)	Found	Recovery (%)
Cabbage	0.122	0.141407	115.907	0.12368	101.3767
	0.238	0.219914	92.40079	0.232927	97.86833
	0.349	0.324919	93.10008	0.353781	101.3698
	0.454	0.476803	105.0227	0.4524	99.64759
Radish	0.122	0.135463	111.0354	0.123071	100.8776
	0.238	0.224478	94.31858	0.235392	98.90438
	0.349	0.334511	95.84847	0.351417	100.6926
	0.454	0.468748	103.2484	0.453384	99.86423
Spinach	0.122	0.136814	112.1428	0.123474	101.2083
	0.238	0.218832	91.94616	0.232551	97.71045
	0.349	0.341841	97.94863	0.355352	101.8201
	0.454	0.465646	102.5652	0.451487	99.44641
Lettuce	0.122	0.13762	112.8036	0.126536	103.7179
	0.238	0.219784	92.34608	0.227125	95.43047
	0.349	0.337109	96.59288	0.356936	102.2739
	0.454	0.468496	103.1929	0.452347	99.63594
Potato	0.122	0.138714	113.7001	0.122151	100.1236
	0.238	0.220223	92.53064	0.234284	98.43881
	0.349	0.332544	95.28475	0.356639	102.1888
	0.454	0.471377	103.8276	0.450243	99.17246
Carrot	0.122	0.134032	109.8621	0.130376	106.8654
	0.238	0.223578	93.94041	0.223099	93.73896
	0.349	0.339949	97.40669	0.352759	101.077
	0.454	0.464978	102.4181	0.456502	100.551
Capsicum	0.122	0.141277	115.8011	0.125801	103.1155
	0.238	0.22032	92.57149	0.229299	96.34406

	0.349	0.324485	92.97578	0.3551	101.7478
	0.454	0.476952	105.0555	0.452964	99.77179
<b>Lake water</b>	0.122	0.141376	115.8819	0.124605	102.1349
	0.238	0.218314	91.72855	0.224347	94.26352
	0.349	0.328372	94.08942	0.369088	105.7558
	0.454	0.475039	104.6341	0.445145	98.04962
<b>Tap water</b>	0.122	0.131606	107.8742	0.124978	102.4408
	0.238	0.225927	94.92723	0.231383	97.21974
	0.349	0.343132	98.31866	0.352793	101.0867
	0.454	0.46212	101.7885	0.453568	99.9049

**Table S2.** Application of the colorimetric readout of sensor system for the determination of  $\text{NO}_3^-$  in real samples spiked with different amounts of  $\text{NO}_3^-$ .

<b>Samples</b>	<b>Added</b>	<b>For sensor CE</b>	
		<b>Found</b>	<b>Recovery (%)</b>
<b>Cabbage</b>	0.122	0.123488	101.22
	0.238	0.235496	98.94795
	0.349	0.350714	100.4911
<b>Radish</b>	0.122	0.129712	106.3212
	0.238	0.222258	93.38563
	0.349	0.357057	102.3085
<b>Spinach</b>	0.122	0.139437	114.293
	0.238	0.202337	85.01568
	0.349	0.367219	105.2202
<b>Lettuce</b>	0.122	0.133771	109.6486
	0.238	0.21384	89.84856
	0.349	0.361312	103.5277
<b>Potato</b>	0.122	0.127916	104.8492
	0.238	0.225819	94.88193
	0.349	0.355195	101.775

<b>Carrot</b>	0.122	0.152742	125.1982
	0.238	0.175199	73.61291
	0.349	0.381122	109.204
<b>Capsicum</b>	0.122	0.12238	100.3113
	0.238	0.237053	99.60225
	0.349	0.349409	100.1171
<b>Lake water</b>	0.122	0.136705	112.0529
	0.238	0.20792	87.36133
	0.349	0.364361	104.4016
<b>Tap water</b>	0.122	0.152656	125.128
	0.238	0.175427	73.70881
	0.349	0.381033	109.1785

**Table S3.** Comparison of chemosensor CF and CE with already reported colorimetric  $\text{NO}_2^-$  and  $\text{NO}_3^-$  sensors based on the Griess assay.

<b>Compound Name</b>	<b>Acid used</b>	<b>LOD</b>	<b>Application</b>	<b>Ref.</b>
p-Aminobenzoyl group modified cellulose thread impregnated with chromotropic acid as a coupling agent.	Sulphuric acid	0.025 mM ( $\text{NO}_2^-$ )	Real sample	[1]
2-naphthylacetic acid-L-phenylalanine-L-phenylalanine hydrogel with sulfanilamide	Phosphoric acid	0.00072 mM ( $\text{NO}_2^-$ )	Real sample	[2]
Griess reagent coated on polystyrene strips with polyethylene glycol	Hydrochloric acid	0.46 mM ( $\text{NO}_2^-$ )	Milk sample Test strips	[3]
Griess reagent modified punched paper on 3D printed support	Hydrochloric acid	0.0017 mM ( $\text{NO}_2^-$ )	Mobile-based sensor, different water sample	[4]
Zn nanoparticles conjugated polyvinylpyrrolidone immobilised on Griess reagent	Hydrochloric acid	0.0062 mM ( $\text{NO}_2^-$ ), 0.137 mM ( $\text{NO}_3^-$ )	Real sample, Test strips	[5]

Immobilisation of Griess reagent on paper	Hydrochloric acid	0.0039 mM (NO <sub>2</sub> <sup>-</sup> )	Mobile-based sensor, water sample	[6]
Carbon dot modified Griess reagent	Hydrochloric acid	0.001 mM (NO <sub>2</sub> <sup>-</sup> )	Real sample,	[7]
Polydimethylsiloxane membranes doped with Griess reagents with dispersed Zn nanoparticles	Citric acid	0.000145 mM (NO <sub>2</sub> <sup>-</sup> ), 0.725 mM (NO <sub>3</sub> <sup>-</sup> )	Real sample analysis, Mobile-based sensor	[8]
CE and CF	Itaconic acid	CE: 0.62 mM (NO <sub>2</sub> <sup>-</sup> ), 2.89 mM; CF: 0.52 mM (NO <sub>3</sub> <sup>-</sup> )	Test kit, Smartphone detection, Environmental samples	This present work

### References:

- 1 P. Singhapphan and F. Unob, Thread-based platform for nitrite detection based on a modified Griess assay, *Sensors Actuators B Chem.*, 2021, **327**, 128938.
- 2 Y.-T. Tai, C.-Y. Cheng, Y.-S. Chen and F.-H. Ko, A hydrogel-based chemosensor applied in conjunction with a Griess assay for real-time colorimetric detection of nitrite in the environment, *Sensors Actuators B Chem.*, 2022, **369**, 132298.
- 3 H. Bharwani, S. Kapur and S. G. Palani, Rapid detection of hydrogen peroxide and nitrite in adulterated cow milk using enzymatic and nonenzymatic methods on a reusable platform, *RSC Adv.*, 2025, **15**, 1577–1589.
- 4 P. Rajasulochana, Y. Ganesan, P. S. Kumar, S. Mahalaxmi, F. Tasneem, M. Ponnuchamy and A. Kapoor, Paper-based microfluidic colorimetric sensor on a 3D printed support for quantitative detection of nitrite in aquatic environments, *Environ. Res.*, 2022, **208**, 112745.
- 5 P. S. Sarvestani, M. Majdinasab, M.-T. Golmakani, S. Shaghaghian and M.-H. Eskandari, Development of a simple and rapid dipstick paper-based test strip for colorimetric determination of nitrate and nitrite in water and foodstuffs, *Food Chem.*, 2024, **461**, 140856.
- 6 D. Gregucci, M. M. Calabretta, F. Nazir, R. J. R. Arias, F. Biondi, R. Desiderio and E. Michelini, An origami colorimetric paper-based sensor for sustainable on-site and instrument-free analysis of nitrite, *Sensors & Diagnostics*, 2025, **4**, 239–246.
- 7 J. Sun, T. Long, Z. Chen, H. Luo, J. Cao, D. Xu and Z. Yuan, Rapid and dual-mode nitrite detection with improved sensitivity by nanointerface-regulated ultrafast Griess assay, *Anal. Chim. Acta*, 2025, **1336**, 343524.
- 8 L. Hakobyan, B. Monforte-Gómez, Y. Moliner-Martínez, C. Molins-Legua and P. Campíns-Falcó, Improving Sustainability of the Griess Reaction by Reagent Stabilization

on PDMS Membranes and ZnNPs as Reductor of Nitrates: Application to Different Water Samples, *Polymers (Basel)*, 2022, **14**, 464.